ΔH is at the upper limit of previous widely varying estimates of the porphyrin-porphyrin interaction.[15] This approach for measuring intramolecular interactions will be discussed in more detail in the following paper, where we introduce the quantities $\Delta\Delta H$ and $\Delta\Delta S$ and extend the same experimental approach to dimers that enclose much larger cavities and afford additional $\pi-\pi$ interactions.[3]

A similar treatment is not possible for the $\pi-\pi$ interaction in $\mathbf{Zn_2 2}$ because the formation of this complex is likely to be associated with an unfavorable strain energy, but we can make an estimate from the kinetic data. Binding by DABCO on the outside of $\mathbf{Zn_2 2}$ cannot lead directly to a complex with DABCO bound inside the cavity. The first and rate-determining step is opening of the cavity (Figure 11). Only then can DABCO bind. Thus the activation energy for this process is the energy required to prise the two porphyrins apart which we estimated above to be 47-51 kJ mol^{-1}. There may be an entropy difference between the closed and open forms and some strain energy may be associated with the open form, so 47 kJ mol^{-1} (11 kcal mol^{-1}) sets an upper limit on the $\pi-\pi$ interaction in this dimer.

We can now rationalize the exchange phenomena observed in the ^{1}H NMR spectrum of free $\mathbf{Zn_2 1}$. An activation energy of 48 kJ mol^{-1} would lead to fast exchange on the ^{1}H NMR time scale at room temperature, and so the meso and racemic forms of $\mathbf{Zn_2 1}$ would appear as an averaged set of signals at room temperature. We do indeed observe fast exchange at room temperature, with an estimated activation energy of 49 kJ mol^{-1} (see above). There may be some entropic and possibly strain contribution to this energy, but, assuming that the major contribution is the $\pi-\pi$ interaction between porphyrins, this agrees with the calculated value of $\Delta H_{\pi\pi}$.

The kinetics of $\mathbf{Zn_2 1}$-DABCO binding indicate that binding of DABCO on the outside of the dimer reduces the strength of the $\pi-\pi$ interaction by at least 8 kJ mol^{-1} (Figure 8), in agreement with previous studies on metalloporphyrin disaggregation by ligands.[6] Pyridine binding to a porphyrin dimer in which there is a strong $\pi-\pi$ interaction reduces the magnitude of the interaction and there is a concomitant reduction in the ligand binding energy relative to binding to a porphyrin monomer. The first binding energy of pyridine to the dimers, $\mathbf{Zn_2 1}$ and $\mathbf{Zn_2 2}$, is reduced by 10 kJ mol^{-1} relative to the energy for binding to **Zn3** (Table II), and we equate this loss in binding energy with a lowering of the porphyrin-porphyrin $\pi-\pi$ interaction. This agrees with our observations for DABCO binding.

Conclusion

We have shown that DABCO can be used to generate a new series of supramolecular porphyrin complexes with defined geometries. The dimers $\mathbf{Zn_2 1}$ and $\mathbf{Zn_2 2}$ show diverse binding properties as a consequence of minor changes in structure, allowing us to probe subtly both the size of the binding pockets and the binding processes. The large variation in behavior we observe such as small two-component systems shows how the high selectivity which occurs in the binding and catalytic properties of multicomponent systems such as enzymes can arise.

We have also used these systems to measure the magnitude of the $\pi-\pi$ interaction between two zinc porphyrins and have investigated the disaggregation effects of ligand coordination on a quantitative level. These measurements along with our previous determination of the geometry of $\pi-\pi$ interactions will enable us to test theoretical models for this poorly understood phenomenon.[4]

Acknowledgment. We thank the DENI (C.A.H.) and SERC (M.N.M. and J.K.M.S.) for financial support.

Thermodynamics of Induced-Fit Binding Inside Polymacrocyclic Porphyrin Hosts

Harry L. Anderson, Christopher A. Hunter, M. Nafees Meah, and Jeremy K. M. Sanders*

Contribution from the Cambridge Center for Molecular Recognition, University Chemical Laboratory, Lensfield Road, Cambridge CB2 1EW, U.K. *Received October 31, 1989*

Abstract: The binding of bis-amine ligands to a series of cyclic zinc porphyrin dimers has been characterized by NMR and electronic spectroscopy. The cavity within the flexible dimers is kept closed by $\pi-\pi$ interactions between the porphyrin and aromatic bridging groups but can be opened by ligands whose binding is strong enough to overcome this energetic barrier. Analysis of the binding of these bifunctional and the corresponding monofunctional ligands to the porphyrin dimers and corresponding monomeric porphyrins allowed definition of the parameters $\Delta\Delta G$, $\Delta\Delta H$, and $\Delta\Delta S$. These are specifically associated with the energetic costs of conformational switching and yield information about the strength of the $\pi-\pi$ interactions that hold the cavity closed. It is estimated that the porphyrin-pyromellitimide $\pi-\pi$ interaction has an energy of 28-56 kJ mol^{-1} (7-13 kcal mol^{-1}), while the porphyrin-biphenyl interaction is ca. 22 kJ mol^{-1} (5 kcal mol^{-1}). A bis-pyridyl porphyrin ligand which has additional recognition sites binds within the cavity with no thermodynamic barrier. It is shown that similar values of $\Delta\Delta G$ can mask radically different binding modes: the values $\Delta\Delta H$ and $\Delta\Delta S$ are more informative, allowing the dissection of the various factors that contribute to or inhibit ligand binding within a cavity.

In the preceding paper[1] we showed how binding studies on the cofacial porphyrin dimers, **1** and **2**, allowed us to measure the $\pi-\pi$ interaction between two porphyrins; we now apply the same techniques to the larger flexible dimeric porphyrin macrocycles, **8**, **9**, and **10**,[2-4] with a view to understanding the more complex intramolecular interactions that control their conformational and binding properties. The relative conformations adopted by the aromatic components of these systems are as illustrated and are

(1) Hunter, C. A.; Meah, N. M.; Sanders, J. K. M., preceding paper in this issue.

(2) We continue the numbering scheme from the preceding paper.

(3) Preliminary communications: Hunter, C. A.; Meah, N. M.; Sanders, J. K. M. *J. Chem. Soc., Chem. Commun.* **1988**, 692-694 and 694-696.

(4) Leighton, P.; Sanders, J. K. M. *J. Chem. Soc., Perkin Trans. I* **1987**, 2385-2393.

0002-7863/90/1512-5780$02.50/0

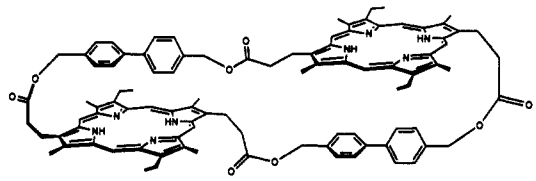

8

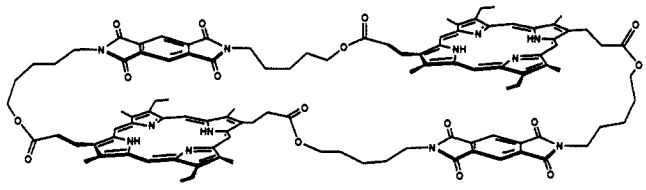

9

controlled by strong $\pi-\pi$ interactions.[5-7] Metalation with zinc does not alter the conformations significantly, although, in the case of Zn_2**9**, it leads to intramolecular coordination between the pyromellitimide carbonyl oxygen and the metal. When Zn_2**8** and Zn_2**9** bind appropriate substrates, global conformational changes are induced (Figure 1).[3] This behavior is analogous to activated-complex binding in induced-fit enzymes: i.e., the enzyme is flexible, and binding the substrates causes a conformational change, which enhances binding of the activated complex.

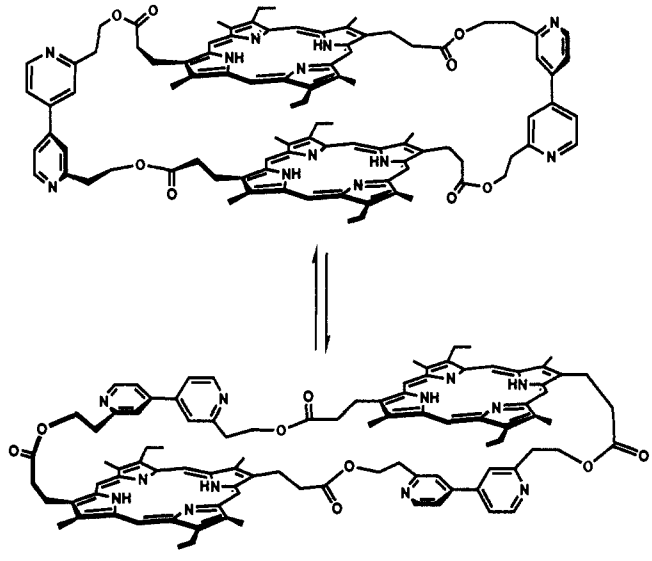

10

These conformational preferences and changes yield qualitative information about the relative magnitudes of the $\pi-\pi$ interactions involved: for example, two porphyrin–pyromellitimide interactions in **9** must be stronger than a porphyrin–porphyrin interaction. The quantitative estimates of $\pi-\pi$ interactions described in this paper have helped us to develop a theoretical model that explains this hitherto poorly understood phenomenon[9] and to design a supramolecular system that exhibits very strong binding of a ligand within a cavity.[10]

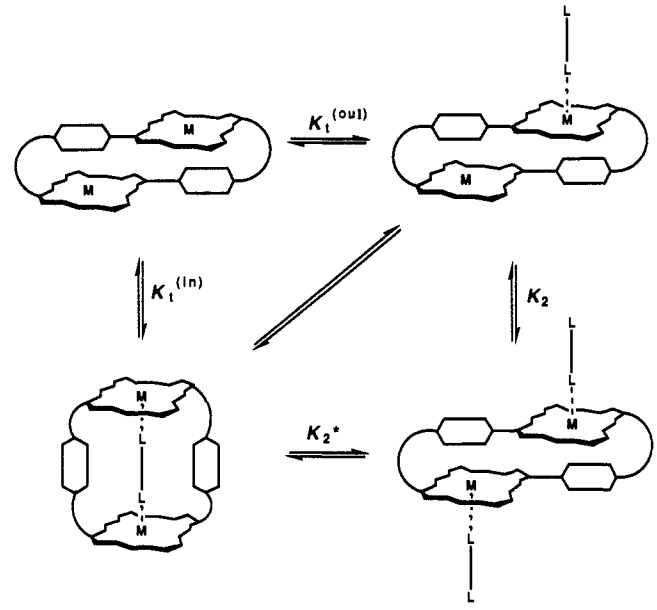

Figure 1. Binding equilibria for reactions between bifunctional ligands and porphyrin dimers.

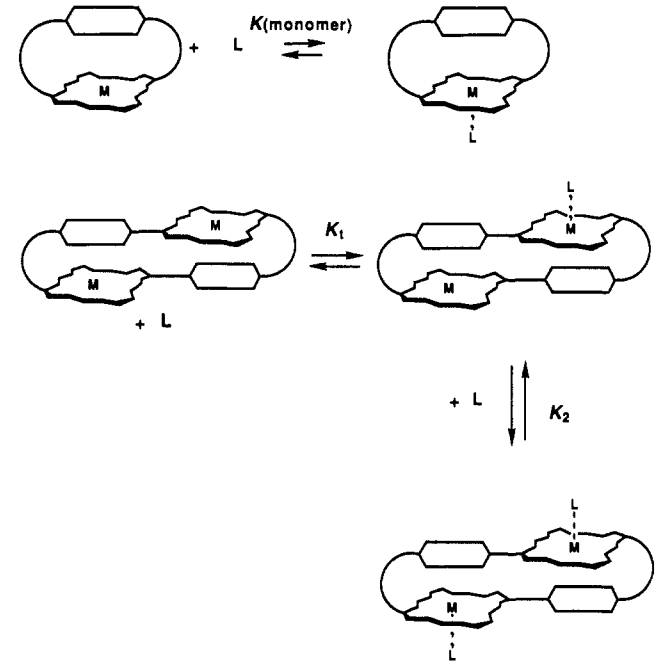

Figure 2. Binding equilibria for reactions between monofunctional ligands and porphyrin dimers.

Approach

We studied the equilibrium between the zinc porphyrin dimers, Zn_2**8** and Zn_2**9**, and the corresponding monomers, **Zn11** and **Zn12**, and a set of mono- and bifunctional ligands, **13–19**. Our ultimate aim is to develop porphyrin-containing molecules that will catalyze reactions between two bound substrates. Monofunctional ligands may be considered as substrate analogues, while bifunctional ligands are analogues for the transition state or intermediate. The present binding studies are a step in the design of artificial enzyme

(5) Evidence for these gross conformations comes from the UV–visible absorption and ^{1}H NMR spectra: the spectra of the dimers **8** and **9** are essentially identical with those of the corresponding capped monomers **11** and **12**.[3] The connecting side chains in all of these compounds are rather flexible, and we have no information on their conformations.

(6) Porphyrin–pyromellitimide conjugates linked by a single flexible chain show essentially the same spectroscopic, binding and stacking behavior as the cyclic dimers: Hunter, C. A.; Sanders, J. K. M. Unpublished results.

(7) The unusual spectroscopic properties[4] of Zn_2**10** indicate an equally populated equilibrium between the two illustrated conformations. The Soret band is split by 14 nm, with one band corresponding to a monomer and the other a π-stacked cofacial dimer.[8] A single conformation with an exciton-split Soret band would give two bands shifted by equal amounts and in opposite directions relative to the corresponding monomer band; the maximum splitting would not exceed 10 nm.[8]

(8) Hunter, C. A.; Sanders, J. K. M.; Stone, A. J. *Chem. Phys.* **1989**, *133*, 395–404.

(9) Hunter, C. A.; Sanders, J. K. M. *J. Am. Chem. Soc.* **1990**, *112*, 5525–5534.

(10) Anderson, H. L.; Hunter, C. A.; Sanders, J. K. M. *J. Chem. Soc., Chem. Commun.* **1989**, 226–227.

Chart I

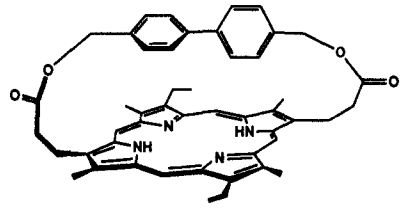

11

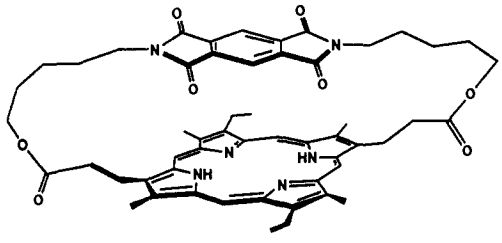

12

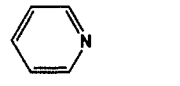

13

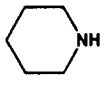

14

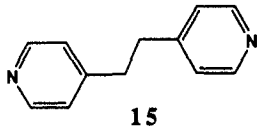

15

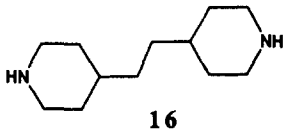

16

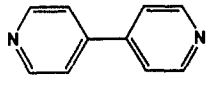

17

18

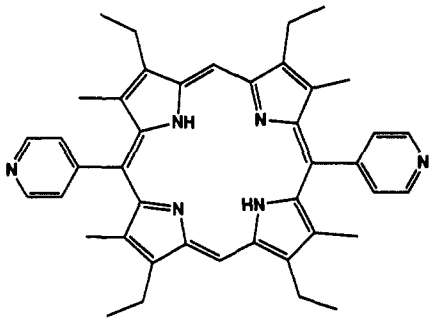

19

systems: if we can assemble a system capable of binding a transition-state analogue (or bifunctional ligand) more strongly than the two corresponding substrates (or monofunctional ligands), then the prospects for catalytic activity are good.

Binding a monofunctional ligand to Zn_2**8** and Zn_2**9** induces essentially no change in the conformation (see later) (Figure 2), because the $\pi-\pi$ interactions still dominate,[9,11] but on binding an appropriate bifunctional ligand global conformational changes occur[3] (Figure 1). The energy required to effect these changes can be measured by comparison of the binding of the same ligands with the corresponding monomeric metalloporphyrins.

Zinc porphyrins generally bind only a single ligand such as pyridine to give a five-coordinate species, and so a monofunctional ligand and a monomeric porphyrin give a 1:1 complex with binding constant K and binding energy $\Delta G = -RT \ln K$ (Figure 3). If the corresponding bifunctional ligand is used, $K_1 \approx 2K$ (Figure 3). However, with a bifunctional ligand there is a second equilibrium possible, which leads to the formation of a 2:1 complex

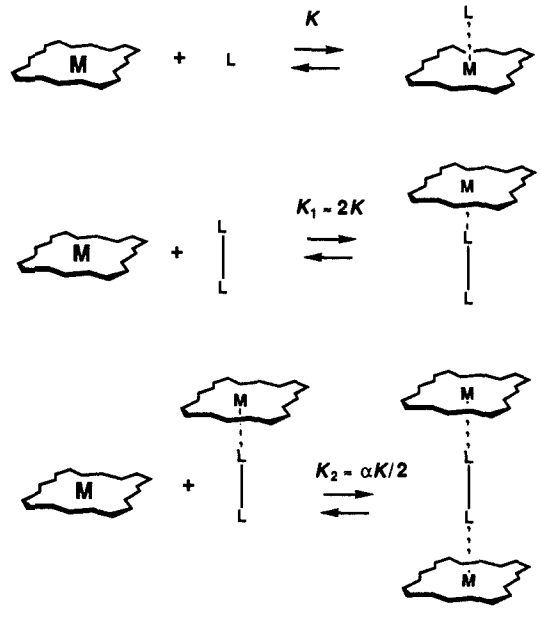

Figure 3. Binding equilibria for reactions between mono- and bifunctional ligands and porphyrin monomers.

(Figure 3); K_1 and K_2 are related by the expression $4K_2 = \alpha K_1$ where α, the interaction parameter, is a measure of the cooperativity between the two ends of the ligand (the statistical factor of 4 takes into account the degeneracy of the monobound species). Similar arguments apply when the situation is reversed and monofunctional ligands bind to dimeric porphyrins (Figure 2). In a noncooperative system, $4K_2 = K_1$; for positive cooperativity, $4K_2 > K_1$ and binding of the first ligand facilitates binding of the second ligand; for negative cooperativity, $4K_2 < K_1$ and binding of the first ligand inhibits binding of the second ligand.[11,12]

The situation is more complicated for equilibria between bifunctional ligands and dimeric porphyrins. The possible equilibria are shown in Figure 1, but usually not all of these equilibria are important, since either binding on the inside or on the outside of the dimer cavity tends to dominate. In most cases only one of the two pathways (either the upper or lower equilibria) need be considered. By using a range of different ligands, we have been able to realize all of the equilibria in Figure 1. The most interesting process is binding of a bifunctional ligand inside the dimer cavity. The binding energy for this process will generally not be twice that for binding of the same ligand to a monomeric porphyrin because there are additional factors. (1) The chelate effect: Binding of a single bifunctional ligand is entropically favored over binding two monofunctional ligands, so the binding constant for a multifunctional ligand is expected to be greater than the product of the binding constants for the separate functionalities.[12] (2) Cooperativity: When one end of the ligand is bound, the basicity of the second site may be lowered, reducing its binding energy. (3) Global conformational changes: Conformational switching induced by ligand binding inside the cavities of these dimers is energetically unfavorable, because $\pi-\pi$ interactions favor the "closed" geometry. (4) New interactions: There may be new interactions in the complex which will alter the binding energy.

To summarize

$$\Delta G(\text{binding inside dimer}) = \Delta G(\text{intrinsic}) + \Delta\Delta G \quad (1)$$

where

$$\Delta G(\text{intrinsic}) = 2\Delta G(\text{monomer binding}) + \Delta G(\text{ligand cooperativity}) \quad (2)$$

(11) Although $\pi-\pi$ interactions are weaker when porphyrins are coordinated by a ligand, they may still control conformation. Hunter, C. A.; Leighton, P.; Sanders, J. K. M. *J. Chem. Soc., Perkin Trans. I* **1989**, 547–552.

(12) Fersht, A. R. *Enzyme Structure and Mechanism*; Freeman: Reading, 1985.

and

$$\Delta\Delta G = \Delta G(\text{chelate effect}) + \Delta G(\text{conformational changes}) + \Delta G(\text{new interactions}) \quad (3)$$

ΔG(intrinsic) can easily be measured:

$$\Delta G(\text{monomer binding}) = -RT \ln \{K(\text{monomer})\} \quad (4)$$

$$\Delta G(\text{ligand cooperativity}) = -RT \ln (\alpha/4) \quad (5)$$

where α is the cooperativity interaction parameter, determined independently as described below. The statistical factor of 4 allows for the degeneracy of the monomeric porphyrin-bifunctional ligand complex. Equation 2 gives

$$\Delta G(\text{intrinsic}) = -RT \ln \{\alpha K^2(\text{monomer})/4\} \quad (6)$$

ΔG(chelate effect) should be approximately constant for all of these systems and can be estimated as follows:

$$\Delta G(\text{chelate effect}) \approx T\Delta S(\text{monomer-monofunctional ligand binding})$$

$$\approx T\Delta S(\text{monomer-bifunctional ligand binding}) - RT \ln 2 \quad (7)$$

So $\Delta\Delta G$, even in these apparently simple systems, is the sum of many different effects. More usefully, it can be factored into the contributing terms $\Delta\Delta H$ and $\Delta\Delta S$, defined as follows, by using eqs 1-7:

$$\Delta\Delta G = \Delta G(\text{dimer binding}) - \Delta G(\text{intrinsic})$$

$$= \Delta H(\text{dimer binding}) - T\Delta S(\text{dimer binding}) - 2\Delta H(\text{monomer binding}) + 2T\Delta S(\text{monomer binding}) + RT \ln (\alpha) - RT \ln 4$$

$$= \Delta G(\text{chelate effect}) + \Delta\Delta H - T\Delta\Delta S \quad (8)$$

where

$$\Delta\Delta H = \Delta H(\text{dimer binding}) - 2\Delta H(\text{monomer binding}) + RT \ln \alpha \quad (9)$$

$$\Delta\Delta S = \Delta S(\text{dimer binding}) - \Delta S(\text{monomer binding}) + R \ln 2 \quad (10)$$

By using these definitions, the only factors which contribute to $\Delta\Delta H$ and $\Delta\Delta S$ are the conformational changes and new interactions in the complexes. These values provide a powerful insight into the nature of the complexes and the interactions which control binding and conformation in these systems. In the previous paper,[1] we used this approach to measure the magnitude of the π–π interaction between two zinc porphyrins: the interaction was equated with $\Delta\Delta H$ for DABCO (1,4-diazabicyclo[2.2.2]octane) binding inside the porphyrin dimer, $\mathbf{Zn_2 1}$.

The concept of $\Delta\Delta G$ is a well-established method for estimating the contribution of a single functional group to the total energy stabilizing a particular molecular conformation,[13,14] but, as we shall show, it should be treated with caution as its value may not bear a simple relation to the behavior of the system studied. Rebek et al. have used this approach to estimate the magnitude of π–π interactions.[14] Sanders et al. have also estimated the magnitude of some porphyrin–aromatic interactions by examining conformational equilibria.[15]

Results

Synthesis. Syntheses of **8**, **9**, and **11** were briefly given previously.[3] Scheme I illustrates an improved, stepwise procedure for **8**; details are given in the Experimental Section. Detailed syntheses of **10** and **12** have been published.[4,16]

Scheme I. Synthesis of Biphenyl Dimer **8**

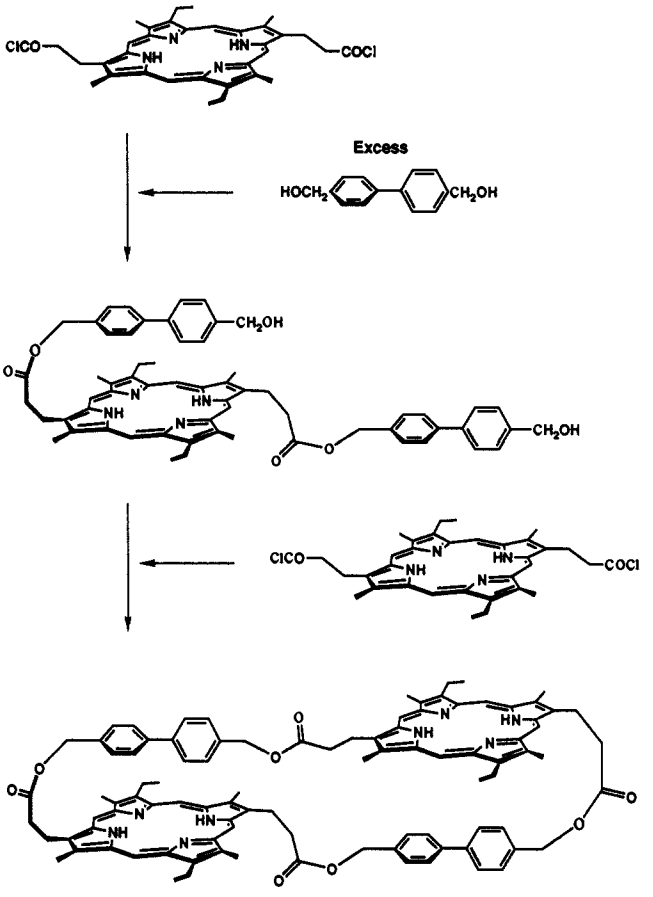

8

Table I. Comparativity in Binding at the Second Site of a Bifunctional Ligand[a]

ligand	K_1/K_2	cooperativity (α)
4	5.2	0.77
16	5.0	0.80
15	5.0	0.80
17	6.4	0.63
19	3.8	1.05

[a] Calculated from the binding constants of the ligands with $\mathbf{Ru^{II}(CO)3}$. All measurements were made on CH_2Cl_2 solutions ca. 10^{-3} M in the ruthenium porphyrin.

Cooperativity in Bifunctional Ligands. We measured the cooperativity coefficient, α, by studying the formation of ternary complexes between bifunctional ligands and monomeric metalloporphyrins.[1] For the metalloporphyrins and ligands of interest, K_2 is too small for ternary complexes to be observed by UV–visible absorption spectroscopy (at 10^{-6} M), and so we used ^{1}H NMR spectroscopy (at 10^{-3} M) to examine the equilibria illustrated in Figure 3. Because the complexes of zinc porphyrins are in fast exchange at room temperature, we have used ruthenium(II) carbonyl mesoporphyrin-II-dimethyl ester, $\mathbf{Ru^{II}(CO)3}$; this forms the corresponding complexes in slow exchange.

^{1}H NMR titrations were carried out by adding the ligand to a solution of the $\mathbf{Ru^{II}(CO)3}$–THF complex in dichloromethane.[17] THF is weakly coordinated and is displaced quantitatively by the nitrogenous bases **13**–**19**. With **15**–**19** the ternary complex was formed initially (Figure 3), and then in the presence of excess ligand the simple 1:1 complex predominated. All the species were

(13) Kellis, J. T., Jr.; Nyberg, K.; Fersht, A. R. *Biochemistry* **1989**, *28*, 4914–22.
(14) Askew, B.; Ballester, P.; Buhr, C.; Jeong, K. S.; Jones, S.; Parris, K.; Williams, K.; Rebek, J., Jr. *J. Am. Chem. Soc.* **1989**, *111*, 1082–1090.
(15) Sanders, G. M.; van Dijk, M.; van Veldhuizen, A.; van der Plas, H. C.; Hofstra, U.; Schaafsma, T. J. *J. Org. Chem.* **1988**, *53*, 5272–5281.
(16) Cowan, J. A.; Sanders, J. K. M. *J. Chem. Soc., Perkin Trans. I* **1985**, 2435–37.
(17) (a) Rillema, D. P.; Nagle, J. K.; Barringer, L. F.; Meyer, T. J. *J. Am. Chem. Soc.* **1981**, *103*, 56–62. (b) Tsutsui, M.; Ostfeld, D.; Hoffman, L. M. *J. Am. Chem. Soc.* **1971**, *93*, 1820–1822.

Table II. Selected ^{1}H NMR Chemical Shifts (in ppm)[a]

porphyrin	ligand	$H_{biphenyl}$[b]		H_{pyro}[c]	H_{meso}		ligand signals		
3					10.06	10.04			
11		3.83	5.49		10.28	10.08			
8		3.91	5.49		10.12	9.94			
12				7.30	10.12	9.74			
9				6.62	10.05	9.79			
Zn3					10.11	10.09			
Zn11		3.94	5.62		10.00	9.88			
Zn_2**8**[d]									
Zn12				6.44	10.04	9.88			
Zn_2**9**				6.07	9.81	9.79			
Zn3	**13**				10.11	10.09			
Zn12	**13**			7.14	10.04	9.66			
Zn_2**8**	**13**	4.46	5.69		10.08	9.90			
Zn_2**8**	**15**	6.98	7.06		9.86	9.85			
Zn_2**8**	**16**	6.8 (br)	6.8 (br)		9.83	9.80	−1.25	−1.61	−3.35
Zn_2**8**	**4**	br	br		9.5 (br)	9.5 (br)	−5.5 (br)		
Zn_2**9**	**13**			6.44	9.99	9.70			
Zn_2**9**	**15**			6.46	9.91	9.71			
Zn_2**9**	**16**			6.79	9.90	9.70	−1.06	−1.30	−2.90
Zn_2**9**	**4**			6.16	9.61	9.32	−5.35		

[a] In $CDCl_3$ solution; br is a broad signal. [b] The chemical shifts of these signals in the biphenyl diol are 7.23 and 7.38 ppm. [c] The chemical shift of this signal in *N,N'*-bis(5-hydroxypentyl)pyromellitimide is 8.25 ppm. [d] Insoluble without a ligand present.

in slow exchange, and, in the presence of more than 0.5 equiv of ligand, free ligand and both the ternary and binary complexes were observed, so that the equilibria in Figure 3 could easily be measured.

$$\frac{K_1}{K_2} = \frac{[Ru^{II}(CO)3\text{–}L]^2}{[Ru^{II}(CO)3\text{–}L\text{–}Ru^{II}(CO)3][L]} \qquad (11)$$

The degree of cooperativity is given by $\alpha = 4K_2/K_1$. From the experimental values of α, listed in Table I, we can see that these ligands show only very weak negative cooperativity. Although complexation to ruthenium has a stronger electronic effect on the ligand than complexation to zinc, the value of α is so close to 1 that to use it for zinc porphyrin complexes should introduce a negligible error in the experiments described below.

^{1}H NMR Spectroscopy. In the absence of added ligand, the ^{1}H NMR spectrum of Zn_2**9** was sharp because of internal coordination of the metal by the pyromellitimide carbonyl groups, but the ^{1}H NMR spectrum of Zn_2**8** was very broad at room temperature because of exchange between several conformations. Addition of monofunctional ligands such as pyridine, **13**, to these dimers yielded spectra which were very similar to those of the free base derivatives.[3] Coordination of pyridine to Zn_2**9** eliminates the intramolecular coordination, and the associated changes in the spectrum are due to a conformational switch from a perpendicular orientation of the π-systems to a parallel "stacked" one (Table II).[18] The spectra of these bis-pyridinate complexes are indicative of the π-stacked conformations illustrated in the structures. The aromatic biphenyl protons of (**13**)$_2$$Zn_2$**8** and H_{pyro} of (**13**)$_2$$Zn_2$**9** show large ring current induced upfield shifts caused by the proximate porphyrin moieties, and one of the porphyrin meso signals is shifted upfield by about 0.3 ppm in the bis-pyridinate complex of Zn_2**9** (Table II).

Addition of 1 equiv of DABCO, **4**, to Zn_2**9** induced a global conformational change, the ligand being bound inside the cavity of the dimer (Figure 4). The ^{1}H NMR spectrum showed the characteristic DABCO methylene signal at −5.35 ppm, shifted upfield by ca. 8 ppm because these protons feel the combined ring currents of both porphyrins.[1] The meso signals appeared at around 9.5 ppm, but the 0.3 ppm separation of these two signals is unusually large compared with other bis-porphyrin–DABCO complexes.[1] This is characteristic of a porphyrin–pyromellitimide π-stacking interaction, indicating that the complex adopts the conformation illustrated in Figure 4. Further evidence supporting this structure is presented below. When more DABCO was added,

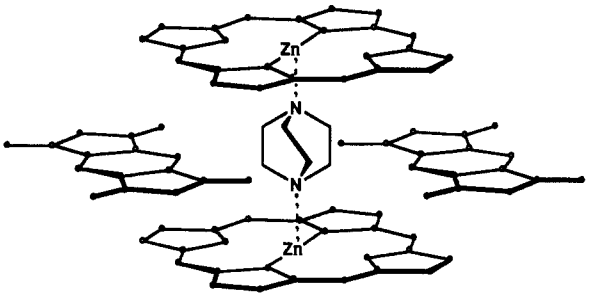

Figure 4. Average conformation of the Zn_2**9**–**4** complex excluding the connecting side chains. These are not shown because there is no information about whether the two porphyrins are rotated 90° relative to each other.

another conformational change was observed. The DABCO signal at −5.35 ppm disappeared, and the porphyrin meso signals moved back downfield to ca. 10.0 and 9.7 ppm, so that spectrum was essentially identical with that of the bis-pyridinate complex. This change is due to binding a second molecule of DABCO: π–π interactions now force a restoration of the initial dimer conformation (Figure 1).

Zn_2**8** showed similar behavior with DABCO: in the presence of 1 equiv of DABCO at 230 K, we observed the characteristic DABCO methylene signal at ca. −5.5 ppm, and the porphyrin meso signals shifted upfield to ca. 9.5 ppm, indicating that DABCO was bound inside the cavity; addition of excess DABCO abolished these shifts, indicating that a second ligand was bound, and so π–π interactions had forced the cavity to collapse as above (Figure 1).

On addition of ca. 4 equiv of **15** to Zn_2**8**, the biphenyl protons of the host shifted from ca. 4.5 and 5.7 ppm to 6.98 and 7.06 ppm, respectively. The ligand signals were in intermediate exchange, so accurate chemical shifts could not be measured. However, at 230 K, we observed the pyridine H_β signal at 5.25 ppm and the H_α signal at 2.92 ppm. Binding of **15** inside Zn_2**8** opens the cavity to its maximum size so the biphenyl groups are completely dissociated from the porphyrins and revert to conventional chemical shifts (Figure 5, Table II). Addition of a large excess of pyridine-d_5 to the **15**–Zn_2**8** complex displaced the bifunctional ligand so that we observed the spectrum of the Zn_2**8** bis-pyridinate complex.

Similar behavior was observed for **15** bound inside Zn_2**9**. However, in this case the ligand is not large enough to extend the cavity to its maximum size, and so there is a residual π–π interaction between the porphyrins and the pyromellitimides. The porphyrin meso signals and H_{pyro} signal show that the two aro-

(18) Harrison, R. J.; Pearce, B.; Beddard, G. S.; Cowan, J. A.; Sanders, J. K. M. *Chem. Phys.* **1987**, *116*, 429–448.

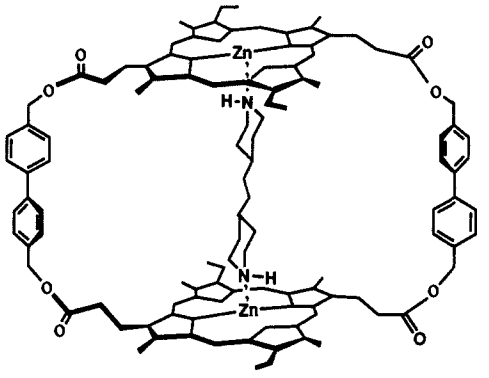

Figure 5. Average conformation of the Zn_2**8–16** complex. The side-chain conformations are purely impressionistic.

matics are still relatively close in space in this complex (Table II).

Similar complexes were formed by **16**: the NMR spectra were in slow exchange at room temperature, and the large upfield shifts in the bound ligand signals showed that it was bound inside the cavity. The ligand opens the cavity of Zn_2**8** to its maximum size (Figure 5), but, like **15**, it is too small to open fully the cavity of Zn_2**9**. There is some residual porphyrin–pyromellitimide π–π interaction in this complex as judged by the 0.2-ppm separation of the meso signals. The H_{pyro} signal of Zn_2**9–16** experiences only a small upfield shift due to the porphyrin ring currents, indicating that the π–π interactions have been moderated.

Further evidence for the conformational preferences in these complexes comes from the measurement of $\Delta\Delta H$ and $\Delta\Delta S$ (see later).

UV–Visible Absorption Spectroscopy. Binding Constants. Binding constants (Table III) were obtained from UV–visible spectrophotometric titrations of the porphyrins with various ligand solutions by using the shift in Soret absorption on ligation.[1] The binding constants for simple systems were obtained from the titration data by using Benesi–Hildebrand plots,[19] and the cooperativity was obtained from Hill plots.[20] However, because of the problems associated with the study of multiple equilibria,[21] we mainly used computer-assisted nonlinear curve-fitting methods for evaluating the titration data.

Some features of the binding constants are in a sense "predictable". All ligands binding to the capped monomeric compounds, **Zn11** and **Zn12**, gave Hill coefficients of 1.00 ± 0.05, indicating the formation of simple 1:1 complexes. The binding of monofunctional ligands to **Zn11** is reduced relative to binding to **Zn3** by 0.35 pK units. This is probably due to blocking of one side of the porphyrin by the cap. The binding constants for **Zn12** are further reduced relative to **Zn3** as a result of the coordination of the pyromellitimide carbonyl oxygen to the metal which competes with ligand binding.[18] Hill coefficients of 1.00 ± 0.05 were obtained for binding of all of the monofunctional ligands to the dimers, Zn_2**8** and Zn_2**9**, apart from pyridine binding to Zn_2**9**. This system showed weak allosteric behavior with a Hill coefficient of 1.14, i.e., the first binding reduces the conformational rigidity of the system and facilitates the second binding. Allosteric behavior is observed only for this weakly bound ligand; for stronger binding ligands, the titration curve is not sensitive to such small differences between the first and second binding constants so $K_1 = 4K_2 \approx 2K$(monomer).[22]

The larger binding constants for the coordination of the bifunctional ligands, with the exception of pyrazine, to the dimers suggest that they are bound predominantly inside the cavity. In the case of DABCO, we observed this process directly in the UV–visible absorption spectrum. During titrations with both dimers, three species were observed: free dimer (Soret λ_{max} 402 nm), dimer with one ligand bound inside the cavity (λ_{max} 409 nm), and dimer with two DABCO ligands attached (λ_{max} 415 nm). DABCO is special in this way because it is the strongest binding ligand and is the only case in which K_2 is large enough to be observed.

For almost all of the other complexes in which the ligand was bound inside the cavity the calculated exciton shift is too small (less than 1 nm) to be seen experimentally. The complexes with **17** bound inside the cavity are predicted to show a blue-shift of 2 nm, but the weak binding of this ligand prevents direct observation of these species. However, curve fitting of the titration data for **17** does provide evidence for such exciton coupling. In contrast to the results for the other ligands, the best fit to the experimental data is obtained if ϵ(1:1 complex bound inside cavity) = 0.85 × ϵ(2:1 complex) (see Experimental Section). This agrees reasonably well with the change in absorbance expected for a 2-nm shift from the maximum of the Soret absorption band.[23] In all other cases, the mono- and bis-bound species cannot be observed independently at 10^{-6} M, and we have assumed that they have identical absorption properties. The measured values of the binding constants, the accuracy of the curve fits obtained by using this assumption, and the ^{1}H NMR data confirm that this is a valid approach.

The titration data for **15** and **16** give Hill coefficients of 1.00 ± 0.05, and the binding constants indicate that the process which we are observing is simply binding inside the cavity to form a 1:1 complex. In general, we expect that K_1(dimer)K_2(dimer) ≈ K^2(monomer), and so K_2 for these systems should be relatively small. Hill coefficients were not measured for **4** as curve fitting was preferred for analyzing the data. The binding of **17** and **18** was more complicated and is discussed in detail below. The values of $\Delta\Delta G$ obtained for the series of ligands are shown in Table IV.

Table III. Binding Constant Data for Zinc Porphyrins (in M^{-1})

porphyrin	ligand	K_1	K_2
Zn11	**13**	1.3×10^3	
Zn11	**14**	1.2×10^4	
Zn11	**18**	1.8×10^2	
Zn11	**17**	1.8×10^3	
Zn11	**15**	4.3×10^3	
Zn11	**16**	3.3×10^4	
Zn11	**4**	4.9×10^4	
Zn_2**8**	**13**	4.1×10^3	1.1×10^3
Zn_2**8**	**14**	3.6×10^4	9.0×10^3
Zn_2**8**	**18**	6.0×10^2	1.5×10^2
Zn_2**8**	**17**	3.8×10^3 [b]	9.5×10^2
Zn_2**8**	**17**	1.3×10^3 [c]	
Zn_2**8**	**15**	5.1×10^5	negligible
Zn_2**8**	**16**	5.1×10^6	negligible
Zn_2**8**	**4**	1.3×10^6	1.3×10^3
Zn12	**13**	3.6×10^2	
Zn12	**14**	4.1×10^3	
Zn12	**18**	4.4×10^1	
Zn12	**17**	7.5×10^2	
Zn12	**15**	1.3×10^3	
Zn12	**16**	1.4×10^4	
Zn12	**4**	2.3×10^4	
Zn12	**19**	1.3×10^3	
Zn_2**9**	**13**	9.6×10^2	3.3×10^2
Zn_2**9**	**14**	8.9×10^3	2.1×10^3
Zn_2**9**	**18**	6.9×10^1	1.7×10^1
Zn_2**9**	**17**	1.8×10^3 [b]	4.6×10^2
Zn_2**9**	**17**	1.0×10^3 [c]	
Zn_2**9**	**15**	3.9×10^3	negligible
Zn_2**9**	**16**	3.9×10^5	negligible
Zn_2**9**	**4**	2.4×10^5	1.0×10^4
Zn_2**9**	**19**	2.6×10^5	negligible
Zn_2**10**	**13**	3.5×10^2	1.8×10^2
Zn_2**10**	**15**	3.4×10^4	negligible

[a] All measurements made on CH_2Cl_2 solutions ca. 10^{-6} M in porphyrin. [b] Outside. [c] Inside.

(19) Benesi, H. A.; Hildebrand, J. H. *J. Am. Chem. Soc.* **1949**, *71*, 2703–2707.
(20) Hill, A. V. *J. Physiol. London* **1910**, *40*, IV–VIII.
(21) (a) Deranleau, D. A. *J. Am. Chem. Soc.* **1969**, *91*, 4050–4054. (b) Person, W. B. *J. Am. Chem. Soc.* **1965**, *87*, 167–170.
(22) Pyrazine binds weakly so binding constants are subject to large errors and allosteric behavior would not be detected with certainty.
(23) The Soret bandwidth was invariably only 11–13 nm in these systems.

Table IV. Values of $\Delta\Delta G$ for Binding Inside Porphyrin Dimers (in kJ mol^{-1})[a]

ligand	porphyrin[a] $Zn_2$8	$Zn_2$9	$Zn_2$10
4	15	15	
16	9	12	
15	5	11	1
17	15	11	
17[b]	15[b]	12[b]	
18			
19		-2	

[a] In CH_2Cl_2 solution. Precision of $\Delta\Delta G$ is estimated to be ±1 kJ mol^{-1}. [b] Value obtained by comparing directly the binding on the outside of the dimer with binding inside the cavity.

Table V. Thermodynamic Data for Ligand Binding to Porphyrins

	ligand 16		4	
porphyrin	ΔS (J K^{-1} mol^{-1})	ΔH (kJ mol^{-1})	ΔS (J K^{-1} mol^{-1})	ΔH (kJ mol^{-1})
Zn11	-120	-60	-120	-60
$Zn_2$8	-120	-70	-230[b]	-100[b]
Zn12	-100	-50	-100	-55
$Zn_2$9	-65	-50	-210	-95

[a] In CH_2Cl_2 solution. Precision is generally estimated to be ±10%. [b] Subject to a large error (ca. ±20%) since very small changes were measured.

Table VI. Estimated Values of $\Delta\Delta H$ and $\Delta\Delta S$ for Binding Inside Porphyrin Dimers

complex[a]	$\Delta\Delta S$ (J K^{-1} mol^{-1})	$\Delta\Delta H$ (kJ mol^{-1})
$Zn_2$8 + 4[b]	-100	20
$Zn_2$8 + 16	0	45
$Zn_2$9 + 4	-110	15
$Zn_2$9 + 16	35	55

[a] In CH_2Cl_2 solution. [b] Subject to a large error since very small changes were measured; errors are ca. ±20%.

Variable-Temperature Experiments. These experiments allow the separation of the entropic and enthalpic contributions to the overall value of $\Delta\Delta G$. The limitation of this approach is that it is only possible to obtain reasonable estimates for the strongly binding ligands, **4** and **16**. The results of the variable temperature UV–visible spectroscopic experiments for these systems are shown in Table V. Table VI lists $\Delta\Delta H$ and $\Delta\Delta S$ for the complexes of the dimers with **4** and **16**. Computer simulation of the variable-temperature titration data with a range of ΔH and ΔS values indicates that, in general, the precision of these values is ± ca. 10%. However, as will be shown below, these large uncertainties still allow identification of the major contribution to $\Delta\Delta G$.

Discussion

We have quantified the thermodynamics of ligand binding to Zn_2**8** and Zn_2**9** by UV–visible spectroscopy and used ^{1}H NMR to probe the geometries of the bound complexes. These results allow us to estimate both the magnitudes and the geometries of the major π-stacking interactions in these systems. By using these observations, we can explain the conformational preferences and binding properties of the two dimers and predict the behavior of other related dimers, such as **10**. In the discussion that follows, we examine each of the dimers and complexes in turn, by using the experimental estimates for $\Delta\Delta H$ and $\Delta\Delta S$ to identify the origins of the various binding and geometry effects observed. It is necessary first, however, to make some general points concerning $\Delta\Delta G$, $\Delta\Delta H$, and $\Delta\Delta S$.

In nearly all the cases described here, $\Delta\Delta G > 0$, i.e., the bifunctional ligands which may be thought of as transition-state analogues are less strongly bound that two of the monomeric ligands (the substrate analogues). In other words, the energetic penalty for global conformational change is greater than the gain in binding energy as a result of the chelate effect and any other favorable interactions. The value of $\Delta\Delta G$ for all of the complexes of Zn_2**8** and Zn_2**9** are relatively uninformative at around 4–10 kJ mol^{-1}. By using eq 7 and the experimentally determined entropy of binding of a monofunctional ligand to a monomeric porphyrin (ca. -120 J K^{-1} mol^{-1}), we estimate ΔG(chelate effect) to be -36 kJ mol^{-1} (-8.6 kcal mol^{-1}) at 300 K. Assuming that there are no new interactions in the complexes, eq 3 implies that the free energy required to open the cavities in these dimers is of the order of 46 kJ mol^{-1} (11 kcal mol^{-1}). However, measurement of $\Delta\Delta H$ and $\Delta\Delta S$ for binding of **4** and **16** to the dimers reveals that the rather uninteresting uniformity in the values of $\Delta\Delta G$ masks radically different types of behavior. $\Delta\Delta H$ and $\Delta\Delta S$ are qualitatively similar for the two dimers and, as we shall show, can be rationalized in terms of the conformations of the complexes (Figures 4 and 5). The only intramolecular interactions that are expected to be important in these systems are π–π interactions, and so the values of $\Delta\Delta H$ reflect to what extent cavity opening has disrupted the bridging group–porphyrin π–π interactions. The values of $\Delta\Delta S$ are simply a measure of the conformational rigidity of the complexes.

The Ligand-Free Dimers. The illustrated geometries of the ligand-free dimers **8** and **9** are controlled by π–π interactions which are generally associated with an interplanar spacing of 3.4–4.0 Å.[9] The shifts of the biphenyl group of **8** suggest that it lies over the center of the porphyrin π-system. In contrast, the relatively small upfield shift in the pyromellitimide ^{1}H NMR signal of **9** suggests an offset geometry for this interaction; the 0.3-ppm upfield shift in one of the meso signals confirms that the pyromellitimide groups tend to lie over the porphyrin periphery rather than over the center. This relatively small shift in the H_{pyro} signal and accompanying upfield shift in one meso signal have been observed in **9**, **12**, and π-stacked monolinked compounds.[6] Further evidence in favor of offset geometries comes from the rates of photoinduced electron transfer from the porphyrin to the pyromellitimide.[18]

For this complex, as for all those described here, the illustration and description of a single conformation is an oversimplification; there will usually be a family of similar conformations for the chromophores, and many conformations for the connecting side chains.

$Zn_2$9–4 Complex. There is a large unfavorable entropy associated with the formation of this complex, suggesting that it has essentially no conformational freedom. The size of $\Delta\Delta S$ is similar to the entropy change for the monofunctional ligand binding to a monomeric porphyrin (-120 J K^{-1} mol^{-1}). In the uncomplexed dimer, the two "stacked" porphyrin–pyromellitimide units are more or less free to move independently of one another, and so the value of $\Delta\Delta S$ indicates that when **4** binds this freedom is lost. The small positive value of $\Delta\Delta H$ for this complex indicates that the π–π interactions have been reduced but not abolished so that there is still some porphyrin–pyromellitimide π-stacking in the bound complex. These results can be explained by the conformation shown in Figure 4: the pyromellitimide groups are folded into the cavity between the two porphyrins, and all the components of the assembly are held in a fixed orientation by π–π interactions.

Further evidence for this conformation comes from NMR: the ring current induced upfield shifts in the 1:1 complex are characteristic of a π-stacking interaction between the pyromellitimide groups and the porphyrins, the meso protons again being strongly nonequivalent. Relative to the bis-pyridine complex of Zn_2**9** (in which there is also a π-stacking interaction), the H_{pyro} signal is shifted upfield by a further 0.3 ppm. Figure 4 indicates that the pyromellitimide groups are sandwiched between the two porphyrins and experience their combined ring currents. This accounts for the additional upfield shift, but the magnitude of the shift is small which suggests that the pyromellitimide groups are slightly displaced from their optimum position by the DABCO.[6] There are four π-stacking interactions in this complex compared with two in the ligand-free dimer, yet $\Delta\Delta H$ is positive: DABCO "blocks" the center of the porphyrin π-systems, slightly changes the geometry of the π–π interaction, and so reduces its magnitude.

$Zn_2$8–4 Complex. This is similar to the Zn_2**9**–**4** complex. The large entropic cost associated with binding suggests a highly

ordered conformation in the complex, but the enthalpic cost is relatively small. The conformation of this complex is thus analogous to that shown in Figure 4, although the biphenyl groups cannot fold fully into the cavity. There is little mobility so $\Delta\Delta S$ is similar to that for the **$Zn_2$9** complex. The small value of $\Delta\Delta H$ reflects a favorable interaction between the π-systems in this geometry.

$Zn_2$8–16 Complex. In contrast to binding of **4**, there is a large enthalpic penalty, but no entropic penalty for binding **16** inside the cavity of **$Zn_2$8**; the complex is less ordered, and the $\pi-\pi$ interactions have been substantially reduced. The NMR results suggest that there is no interaction between the biphenyl groups and the porphyrins in the complex. Figure 5 illustrates the conformation of the **$Zn_2$8–16** complex; the $\pi-\pi$ interactions have been abolished, and the bridging groups have significant mobility. The conformational freedom in this complex is similar to that in the uncomplexed dimer so $\Delta\Delta S \approx 0$. The enthalpic cost of opening the cavity, 44 kJ mol^{-1}, arises from disruption of the $\pi-\pi$ interactions: assuming that there is no residual $\pi-\pi$ interaction in the complex, we estimate that the porphyrin–biphenyl interaction is worth ca. 22 kJ mol^{-1} (5 kcal mol^{-1}).[24]

$Zn_2$9–16 Complex. Similarly, **16** significantly disrupts the $\pi-\pi$ interactions in **$Zn_2$9**, but the ^{1}H NMR results indicate that they are not fully abolished. The conformation of this complex is similar to that shown in Figure 5 except that the longer flexible chains which link the pyromellitimide and porphyrin units allow a limited amount of $\pi-\pi$ interaction. Thus the $\Delta\Delta H$ of 56 kJ mol^{-1} gives lower limit of 28 kJ mol^{-1} (7 kcal mol^{-1}) for the porphyrin–pyromellitimide $\pi-\pi$ interaction.[25] There is a great deal of conformational freedom associated with this complex: the aromatic components are not fixed in place by strong $\pi-\pi$ interactions, and the ligand does not extend the cavity to its maximum size so that the bridging groups are very mobile and $\Delta\Delta S$ is positive.

$Zn_2$8–15 Complex. This complex has a smaller value of $\Delta\Delta G$ than any of the other complexes of **$Zn_2$8** and **$Zn_2$9**. ^{1}H NMR suggests that the geometry of the complex is essentially identical with that of the **$Zn_2$8–16** complex in which the ligand is the saturated analogue of **15**. There may be favorable $\pi-\pi$ interactions between the biphenyl bridges and the ligand in this complex which lower the energetic cost of binding inside the cavity.

Complexes with 18. Pyrazine, **18**, is a weakly binding ligand. The energy of binding the second end of the ligand is less than the energy required for the conformational change (ca. 46 kJ mol^{-1}), so pyrazine binds exclusively on the outside of the dimers (upper equilibria in Figure 1).

Complexes with 17. Here the energy of binding the second end of the ligand is comparable to the energy required for cavity opening, giving an equilibrium between binding on the inside and outside of the dimer. Hill plots of the titration data for **17** yielded a slope of 0.90 for binding to **$Zn_2$8** and 0.85 for binding to **$Zn_2$9**: binding of the first ligand inside the cavity inhibits binding of the second ligand. Such inhibition also occurs in the other systems we have studied, but binding inside the cavity was so strong that the second ligand binding was too small to be significant at the concentrations of interest. By using computer-aided curve-fitting routines, neither the equation for binding a single ligand nor the equation for binding two identical ligands gave good fits to the experimental curves for **17** binding, and it was necessary to take the inside–outside equilibrium into account (see Experimental Section).

Implications. Comparison of these values for $\pi-\pi$ interactions with the 48 kJ mol^{-1} measured for the zinc porphyrin–zinc porphyrin $\pi-\pi$ interaction[1] explains the conformations adopted by the dimers **8**, **9**, and **10**. In **9**, the two pyromellitimide–porphyrin interactions (28–56 kJ mol^{-1} each) are stronger than one porphyrin–porphyrin interaction and so dominate. In **8**, the side chains do not allow the two porphyrins to stack, and so the attractive porphyrin–biphenyl interaction controls the conformation. If the energy of the porphyrin–bipyridyl interaction is similar to the porphyrin–biphenyl interaction (22 kJ mol^{-1} each), then, in **10**, the porphyrin–porphyrin interaction will be of a similar order of magnitude to two porphyrin–bipyridyl interactions, explaining the equilibrium between two different π-stacked conformations (see structures).

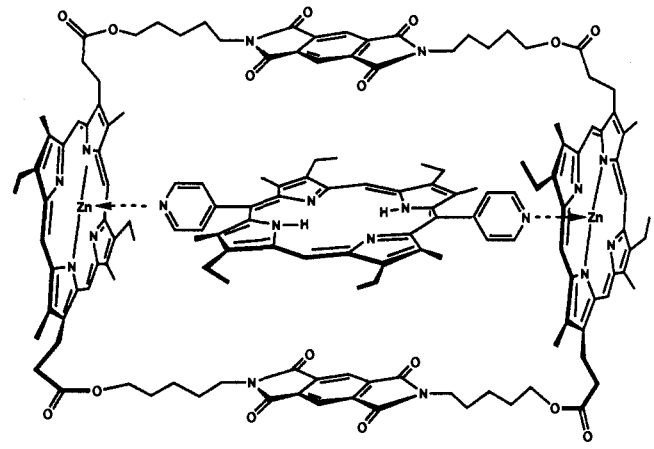

Figure 6. Average conformation of the **$Zn_2$9–19** complex. The side-chain conformations are purely impressionistic.

We have shown that it is possible to rationalize conformational changes and binding between two species, which have multiple recognition sites, in terms of the sum of the entropic and enthalpic contributions of each individual interaction to the overall binding energy. Having measured all the important interactions in these porphyrin systems, we should be able to predict how the binding properties will change if we modify the dominant $\pi-\pi$ interactions or introduce some new recognition sites. Consider, for example, binding of a bifunctional ligand, **15**, inside **$Zn_2$10**. The cavity inside **$Zn_2$10** is similar in size to the **$Zn_2$8** cavity, and the magnitudes of the $\pi-\pi$ interactions which control the conformations of the ligand-free dimers are also comparable. However, pyridine (**13**) binding to **$Zn_2$10** causes a significant disruption of the $\pi-\pi$ interactions (cf. the cofacial dimers, **$Zn_2$1** and **$Zn_2$2**):[11] the total binding energy is 10.7 kJ mol^{-1} less than that for pyridine binding to **$Zn_2$8** (Table III). Thus we expect the energetic cost of opening the **$Zn_2$10** cavity to be somewhat less than that for opening **$Zn_2$8**.[24] The value of $\Delta\Delta G$ for binding **15** confirms this prediction (Table IV).

More importantly, we can lower the energetic cost of binding inside the cavity of a dimer by introducing additional recognition sites. Binding of **19** inside **$Zn_2$9** is an example of this, the extra recognition sites being $\pi-\pi$ interactions between the ligand and the side walls of the cavity. Figure 6 illustrates the conformation of this complex as determined by ^{1}H NMR spectroscopy.[10] In this complex there are two porphyrin–pyromellitimide $\pi-\pi$ interactions, and so overall there is no loss in $\pi-\pi$ interaction and we expect that $\Delta\Delta H \approx 0$. The entire supramolecular assembly is held rigid so that $\Delta\Delta S$ should be around -120 J K^{-1} mol^{-1}, as in **$Zn_2$9–4**. Combining these parameters, we predict $\Delta\Delta G \approx 0$, which is indeed experimentally observed (Table IV).[26]

A comparison of the **15–$Zn_2$9** and **19–$Zn_2$9** binding constants demonstrates that incorporation of additional $\pi-\pi$ interactions into these host–guest complexes can enhance binding by two orders of magnitude, despite the unfavorable entropic contributions associated with such interactions. Systems which are properly designed to incorporate such interactions at no entropic cost should show dramatically enhanced binding properties with appropriate substrates.

(24) Our definition of $\Delta\Delta H$ estimates the magnitude of the $\pi-\pi$ interaction between a ligated zinc porphyrin and the bridging π-system. Ligand coordination reduces $\pi-\pi$ interactions between porphyrins so the magnitude of the interaction in the uncomplexed species is likely to be larger.[8]

(25) We obtain an upper limit for this interaction of 56 kJ mol^{-1} from competition experiments between pyridine binding and π-stacking.[6]

(26) The binding constant for the **Zn12–19** complex could not be measured reliably. However, titration results show that it is of the same order of magnitude as for pyridine, and we have used the value for **Zn12–15** binding to estimate $\Delta\Delta G$ for the **$Zn_2$9–19** complex.

Conclusion

We have shown that a quantitative measure of inter- and intramolecular interactions can help in developing an understanding of the conformations and properties of supramolecular systems. Our results provide an insight into the important features of the thermodynamics of conformational switching and the behavior of induced-fit enzyme models. The value $\Delta\Delta G$, as defined here, should prove useful for the predicting of the potential catalytic properties of porphyrin dimers; the values measured for these flexible systems are all positive, so we do not expect them to catalyze bimolecular reactions.[27] However, in the analysis of intra- and intermolecular interactions, we suggest that $\Delta\Delta G$ should be avoided where possible. Even for the apparently simple complexes studied here, $\Delta\Delta G$ bears little relation to the mode of binding: the values $\Delta\Delta H$ and $\Delta\Delta S$ are much more useful. In a related paper,[9] we use the values measured for $\pi-\pi$ interactions to develop a simple theoretical model.

Experimental Section

UV-vis electronic absorption spectra were recorded on dichloromethane solutions, ca. 10^{-6} M in porphyrin, by using a Pye Unicam PU 8800 spectrometer with variable temperature facility. For titrations the apparatus was rigorously cleaned and dried, and the dichloromethane was distilled from calcium hydride. Accurately determined ligand solutions were made up in 1-mL volumetric flasks. They were added to the porphyrin samples in 1-5-μL aliquots via a 10-μL Hamilton 800 Series syringe. The analysis of the results allowed for the changes in volume during the titration. For variable-temperature UV-vis experiments, accurately measured mixed ligand-porphyrin solutions were made up such that the ratio of free/bound porphyrin was ca. 1. The absorbance of this mixture was recorded at two wavelengths (usually the absorption maxima of the free and bound species) and at 20 different temperatures in the range 0-35 °C. Titration and variable-temperature data were analyzed on a Macintosh SE microcomputer by graphical and curve-fitting programs; the latter are based on Simplex routines written by Dr. A. Crawford.

Nuclear magnetic resonance spectra of deuteriochloroform or deuteriodichloromethane solutions were recorded on a Bruker AM-400 spectrometer. Data were accumulated over 16K or 32K data points with a spectral width of 12 or 20 ppm. FAB mass spectra were obtained on an MS 30 instrument.

In reactions involving porphyrin esterifications, air and water were rigorously excluded: apparatus was baked at 550 K for 24 h before use, and reagents and solvents were dried. Reagents were kept under positive pressure of dry nitrogen during reaction and transfers; the porphyrin acid chloride is light-sensitive, so reaction vessels were covered with aluminum foil. Product porphyrins were metalated by using $Zn(OAc)_2$ by standard procedures.[28]

Pyromellitimide Dimer 9 and Capped Monomer 12. Mesoporphyrin-II-diacid (190 mg, 0.33 mmol) was dispersed in dry dichloromethane (50 mL). Oxalyl chloride (1.5 mL) and DMF (1 drop) were added, and the mixture was stirred in the dark for 1 h to give a clear pink solution. Solvent and excess oxalyl chloride were removed under reduced pressure to yield mesoporphyrin-II-diacid chloride as a purple gum. This was dissolved in dichloromethane (250 mL) and transferred via a stainless steel cannula to a dropping funnel.

N,N'-bis(5-hydroxypentyl)pyromellitimide (130 mg, 0.33 mmol)[16] was similarly dissolved in a mixture of dry DMF (50 mL) and dry dichloromethane (200 mL) and transferred to an identical dropping funnel. These two solutions were added with stirring to a solution of freshly recrystallized *N*-(dimethylamino)pyridine (DMAP) (0.7 g) in dry dichloromethane (100 mL) over 8 h. The reaction mixture was stirred for a further 12 h. The solvent was then evaporated under reduced pressure. The purple residue was dissolved in dichloromethane (ca. 50 mL) and filtered through a short column of Fluorisil to remove polymers and DMAP hydrochloride. The solution was washed with 0.1 M hydrochloric acid to remove residual DMAP and then with water. The organic layer, after drying with magnesium sulfate, was flash chromatographed on silica with dichloromethane–5% methanol eluant. The first band eluted was a mixture of **12** and **9**.

The products were separated by preparative TLC, eluting with CH_2Cl_2–2% methanol. The first major band was identical in its UV-vis, NMR, and mass spectra to authentic[16] capped monomer **12**. It was recrystallized from CH_2Cl_2–hexane giving a purple powder (110 mg, 36%). The second major band was the dimeric product, **9**. It was recrystallized from CH_2Cl_2–hexane giving a purple powder (18 mg, 12%). NMR ($CDCl_3$) 10.05 (4 H, s, meso), 9.79 (4 H, s, meso), 6.62 (4 H, s, Ar-*H*), 4.0–4.2 (24 H, br, m, porph-CH_2 and O-CH_2), 3.62 (12 H, s, porph-CH_3), 3.58 (12 H, s, porph-CH_3), 3.19 (8 H, t, OC-CH_2), 1.93 (12 H, t, porph-CH_2-CH_3); 1.31 (br, m, pyromellitimide bridge CH_2), 0.7–0.9 (br, m, pyromellitimide bridge CH_2), –4.21 (4 H, s, NH); UV-vis 399, 500, 534, 569, 623 nm; *m/z* 1837 (MH^+); $C_{108}H_{116}O_{16}N_{12}$ requires M^+ = 1836.

Biphenyl Dimer 8 and Capped Monomer 11. Mesoporphyrin-II-diacid (150 mg, 0.26 mmol) was converted to the acid chloride as above, dissolved in dry dichloromethane (50 mL), and transferred to a dropping funnel. 4,4'-Dibenzyl diol (650 mg, 3.0 mmol) and DMAP (100 mg, 0.8 mmol) were dissolved in DMF (50 mL) and transferred to the reaction vessel. The acid chloride solution was added with stirring over 8 h. The reaction mixture was stirred for a further 12 h.

The solvent was then evaporated under reduced pressure. The purple residue was dissolved in dichloromethane (ca. 50 mL) and washed with 0.1 M hydrochloric acid to remove residual DMAP and then with water. The organic layer, after drying with magnesium sulfate, was flash chromatographed on silica with CH_2Cl_2–5% methanol eluant. The first band eluted was the capped monomer, **11**, and the second band was meso-porphyrin-II bis(4,4'-dibenzyl) diester diol **20**. The products were purified by preparative TLC. The diol (60 mg, 24%) was used for the next stage of dimer syntesis. **11** was recrystallized from CH_2Cl_2–hexane giving purple crystals (24 mg, 12%). NMR ($CDCl_3$) 10.28 (2 H, s meso), 10.08 (2 H, s, meso), 5.49 (4 H, d, biphenyl H), 5.04 (2 H, d, biphenyl-CH_2), 4.68 (2 H, d, biphenyl-CH_2), 4.5 (4 H, t, porph-CH_2CH$_2$), 4.08 (4 H, q, porph-CH_2CH$_3$), 3.83 (4 H, d, biphenyl H), 3.67 (12 H, s, porph-CH_3), 3.35 (8 H, t, OC-CH_2), 1.83 (6 H, t, porph-CH_2-CH_3), –3.8 (4 H, s, NH); UV-vis 400, 500, 532, 568, 622 nm; *m/z* 745 (MH^+); $C_{48}H_{48}O_4N_4$ requires M^+ = 744.

Mesoporphyrin-II-diacid (50 mg, 0.09 mmol) was converted to the acid chloride as above, dissolved in dichloromethane (125 mL), and transferred to a dropping funnel. The meso-porphyrin-II bis(4,4'-dibenzyl) diester diol **20** (60 mg, 0.06 mmol) was similarly dissolved in dichloromethane (125 mL) and transferred to a funnel. The two solutions were added with stirring to a solution of freshly recrystallized DMAP (100 mg, 0.8 mmol) in dry dichloromethane (250 mL) over 6 h. The reaction mixture was stirred for a further 12 h. The solvent was then evaporated under reduced pressure. The resultant purple solid was dissolved in dichloromethane (ca. 50 mL) and filtered through Fluorisil. The solution was then washed with 0.1 M hydrochloric acid and then with water. The organic layer, after drying with magnesium sulfate, was flash chromatographed on silica with dichloromethane–5% methanol eluant. The first band eluted was the dimer **8**. The product was purified by preparative TLC, eluting with CH_2Cl_2–2% methanol. It was recrystallized from CH_2Cl_2–hexane giving a purple powder (40 mg, 44%). NMR ($CDCl_3$) 10.12 (4 H, s, meso), 9.94 (4 H, s, meso), 5.49 (8 H, d, biphenyl H), 4.78 (biphenyl-CH_2), 4.5 (8 H, t, porph-CH_2CH$_2$), 3.91 (8 H, d, biphenyl H), 3.94 (8 H, q, porph-CH_2CH$_3$), 3.56 (24 H, s, porph-CH_3), 3.35 (8 H, t, OC-CH_2), 1.65 (12 H, t, porph-CH_2-CH_3), –3.8 (4 H, s, NH); UV-vis 400, 500, 532, 568, 622 nm; *m/z* 1489 (MH^+); $C_{96}H_{96}O_8N_8$ requires M^+ = 1488.

5,15-Bis(4-pyridyl)-2,8,12,18-tetraethyl-3,7,13,17-tetramethylporphyrin (19).[29] *p*-Toluenesulfonic acid monohydrate (207 mg) was added to a solution of 3,3'-diethyl-4,4'-dimethyldipyrromethane (250 mg, 1.09 mmol) and 4-pyridinecarboxaldehyde (103 μL, 1.09 mmol) in methanol (20 mL). The mixture was deoxygenated and stirred under argon for 24 h. The solvent was removed by evaporation, and the crude porphyrinogen was dissolved in THF (20 mL), stirred with DDQ (740 mg, 3.27 mmol) for 4 h, evaporated, redissolved in 10% MeOH/$CHCl_3$, and eluted through a silica column with this solvent. The fastest band was collected, evaporated to 10 mL, and crystallized by addition of methanol (60 mL). The dark red crystals were filtered off and dried in vacuo, overall yield, 230 mg (67%): NMR ($CDCl_3$/CD_3OD) 10.15 (2 H, s, meso), 8.82 (4 H, d, α-Py), 7.99 (4 H, d, β-Py), 3.87 (8 H, q, porph-CH_2-CH$_3$), 2.36 (12 H, s, porph-CH_3), 1.62 (12 H, t, porph-CH_2-CH_3); UV-vis 406, 505, 540, 572, 625 nm; *m/z* 632 (M^+); $C_{42}H_{44}N_6$ requires M^+ = 632.

Mesoporphyrin-II-dimethyl Ester Ruthenium Carbonyl THF Complex (Ru^{II}(CO)3-THF).[17] A mixture of mesoporphyrin-II-dimethyl ester (50 mg, 84 mmol), triruthenium dodecacarbonyl (60 mg, 94 mmol), and decalin (10 mL) was deoxygenated, saturated with argon, and refluxed under argon, in darkness, for 3 h. The mixture was cooled, THF (1 mL) was added, and then the pressure was reduced to remove all solvent at

(27) For rigid porphyrin systems that bind the second ligand with negative $\Delta\Delta G$ see: (a) Anderson, H. L.; Sanders, J. K. M. *J. Chem. Soc., Chem. Commun.* **1989**, 1715–1716. (b) Danks, I. P.; Sutherland, I. O.; Yap, C. H. *J. Chem. Soc., Perkin Trans. I* **1990**, 421–422.

(28) Buchler, J. W. *The Porphyrins, Vol. I*; Dolphin, D., Ed.; Academic Press: New York, 1978; pp 390–474.

(29) Gunter, M. J.; Mander, L. N. *J. Org. Chem.* **1981**, *46*, 4792–4794.

room temperature. The dark brown residue was dissolved in 1:1 THF/CH_2Cl_2 (40 mL), filtered to remove ruthenium metal, evaporated, columned through SiO_2 (eluting with 1% THF/CH_2Cl_2), and evaporated to yield copper red crystals (62 mg, 93%). NMR (CD_2Cl_2) 9.97 (2 H, s), 9.94 (2 H, s), 4.34 (4 H, t), 4.04 (4 H, q), 3.64 (6 H, s), 3.60 (6 H, s), 3.59 (6 H, s), 3.28 (4 H, t), 1.89 (6 H, t), 1.03 (4 H, br s), 0.11 (4 H, br s); UV-vis 390, 516, 548 nm; IR ν_{CO} (CH_2Cl_2) 1928 cm^{-1}; m/z isotopic distributions centered on 722.4 (M^+) and 694.4 ($M - CO^+$); $C_{37}H_{40}O_5N_4Ru$ requires M^+ = 721.9 and $C_{36}H_{40}O_4N_4Ru$ requires M^+ = 693.9.

Analysis of Titration Data. In the titrations it is not possible to measure independently the absorption of the 1:1 and 2:1 complexes for the monofunctional ligands binding to the dimers. This can lead to interpretation errors when dealing with sequential binding at a single site,[21] but we have two separate sites whose properties are identical. As a starting point we assumed that to a good approximation, the extinction coefficients of the 1:1 complexes at any wavelength are given by

$$\epsilon(1{:}1\ \text{complex}) = 0.5\ \epsilon(\text{free dimer}) + 0.5\ \epsilon(2{:}1\ \text{complex}) \quad (12)$$

The absorption of the dimer is in effect the sum of the absorptions of the two porphyrin units. Justification for this assumption comes from curve-fitting routines: using the above values for the 1:1 complex extinction coefficients yields a much better fit to the data than any other values. For bifunctional ligands we assumed

$$\epsilon(1{:}1\ \text{complex bound inside cavity}) = \epsilon(2{:}1\ \text{complex}) \quad (13)$$

This is reasonable where the degree of exciton coupling is negligible. With DABCO, **4**, the 1:1 complex is observable directly, and no assumptions are required; with 4,4'-dipyridyl **17** an additional factor of 0.85 gave the best fit (see Results). The following equation and the titration data were used to determine if there was cooperativity in binding to the dimers:

$$\ln\{(A - A_0)/(A_f - A)\} = x \ln [\text{free ligand}] + \ln K \quad (14)$$

where A is the absorption at a particular wavelength, λ; A_0 is the initial absorption at λ; A_f is the final absorption at λ; K is the binding constant; and x is a constant which defines the number of ligands bound per site. A plot of $\ln\{(A - A_0)/(A_f - A)\}$ vs ln [free ligand] yields a straight line of slope 1 for independent, identical binding at the two sites. Cooperative binding, where the second binding is aided by the first, gives $x > 1$, while negative cooperativity gives $x < 1$.

The data were also analyzed by using a least-squares curve-fitting routine. For systems exhibiting cooperativity this was essential in order to obtain accurate binding constants; in simpler systems, these curve-fitting results merely confirmed those obtained by the above analysis. The data were analyzed by using the expression

$$A = \frac{A_0 + K_1[L]A_1 + K_1K_2[L]^2A_2}{1 + K_1[L] + K_1K_2[L]} \quad (15)$$

where A_0 = absorbance for free dimer at λ; A_1 = absorbance for 1:1 complex at λ; A_2 = absorbance for 2:1 complex at λ. The other symbols have the same meaning as above. The expression

$$A = \frac{A_0 + K_1^{out}[L]\{0.5A_0 + 0.5A_2\} + K_1^{in}[L]0.85A_2 + 0.5(K_1^{out})^2[L]^2A_2}{1 + K_1^{out}[L] + K_1^{in}[L] + 0.5(K_1^{out})^2[L]^2} \quad (16)$$

was used to fit the data from the titrations of **17** to take into account the equilibrium between binding on the outside and on the inside of the dimers in the 1:1 complexes. This equation (less the correction factor of 0.85) also fitted the data for the other ligands and confirmed that, over most of the titration, all except pyrazine were bound exclusively inside the cavity.

Acknowledgment. We thank the SERC (UK) and Department of Education (Northern Ireland) for financial support and Dr. A. Crawford for the Simplex routines.

Electron Paramagnetic Resonance and Electrochemical Study of the Oxidation Chemistry of Mononuclear and Binuclear Chromium Carbonyl Thiolates†

Jerry Springs,‡ Christopher P. Janzen,‡ Marcetta Y. Darensbourg,*,‡ Joseph C. Calabrese,§ Paul J. Krusic,*,§ Jean-Noël Verpeaux,∥ and Christian Amatore*,∥

Contribution from the Department of Chemistry, Texas A&M University, College Station, Texas 77843, the Central Research and Development Department, E. I. du Pont de Nemours and Company, Experimental Station, Wilmington, Delaware 19880-0328, and the Laboratoire de Chimie (CNRS-UA 1110), Ecole Normale Supérieure, 75231 Paris Cedex 05, France.
Received November 27, 1989

Abstract: The oxidation chemistry of $RSCr(CO)_5^-$ thiolate anions, $1(R)^-$, and of their binuclear analogues $RS[Cr(CO)_5]_2^-$, $2(R)^-$, has been studied by cyclic voltammetry, EPR, and low-temperature IR. Rapid potential scan cyclic voltammetry shows that the radicals $1(R)^\bullet$ have lifetimes of less than 50 μs and decay by first-order kinetics. Chemical studies are consistent with fragmentation of $1(R)^\bullet$ into an alkylthiyl radical $RS^\bullet$ and a $Cr(CO)_5$ fragment. The slower reactions following the initial irreversible oxidation have been elucidated by cyclic voltammetry. The major product of chemical and electrochemical oxidation of $1(R)^-$ is the monodentate disulfide complex $(RS-SR)Cr(CO)_5$ formed by complexation of $Cr(CO)_5$ fragments to the organic disulfide resulting from dimerization of $RS^\bullet$ radicals. The electrochemical oxidation of $2(R)^-$ proceeds in two chemically reversible steps to the corresponding $2(R)^\bullet$ radicals and $2(R)^+$ sulfonium cations. The intensely colored $2(R)^\bullet$ radicals have limited thermal stability and were characterized by EPR, low-temperature IR, and extended Hückel MO calculations. The unpaired electron resides to a large extent in a p-type orbital on the trigonal sulfur, which is π-conjugated to d orbitals of the neighboring Cr atoms. This orbital is part of a three-center pseudoallylic π system occupied by five electrons, totally analogous to that with four-electron occupancy put forward previously for binuclear phosphinidene complexes $RP[ML_n]_2$, e.g., $RP[Cr(CO)_5]_2$, which is isoelectronic with $2(R)^+$. The X-ray structures of t-$BuSCr(CO)_5^-$ and t-$BuS[Cr(CO)_5]_2^-$ are also presented.

Introduction

Although most well-known chemical reactions of transition-metal complexes involve transformations occurring at the metal center, ligand-centered reactions can offer important alternative features of reactivity. Transition-metal thiolato complexes, supported by carbonyl ligands, offer an opportunity to examine ligand- vs metal-based reactivity, both by experiment and theory. For example, the Fe(II) complexes $(\eta^5\text{-}C_5H_5)Fe(CO)_2(SAr)$ (Ar = C_6H_5 and $p\text{-}C_6H_4X$) have been shown to be chemically active toward nucleophiles via sulfur lone-pair reactivity in accord with

† Du Pont contribution no. 5354.
‡ Texas A&M University.
§ E. I. du Pont de Nemours and Co.
∥ Ecole Normale Supérieure.

0002-7863/90/1512-5789$02.50/0